



Dynamic behaviour of cavitation clouds: visualization and statistical analysis

Ezddin Hutli^{1,2,3} · Milos Nedeljkovic⁴ · Attila Bonyár⁵

Received: 21 January 2019 / Accepted: 25 May 2019 / Published online: 8 June 2019
© The Author(s) 2019

Abstract

High-speed visualization and subsequent statistical analysis of a high-speed cavitating water jet were performed with a custom image acquisition and processing system. In a cavitating water jet, cavity clouds form and collapse with an unsteady, periodic tendency where the frequency depends on the flow conditions. The aim of the presented investigations was to examine and analyse the dynamic behaviour of these cavity clouds to understand the effect of the influencing experimental working conditions, such as injection pressure, nozzle geometry and shape (convergent or divergent) on the size, integrity and life cycle of the clouds. The results show oscillation patterns in the geometry of the clouds (thickness, length, area, etc.), through shedding, growing, shrinking, which are related to upstream pressure fluctuations caused by the plunger pump and the interaction between the jet and the surroundings. The corresponding characteristic oscillation frequencies of the cavitating jets were also determined through cloud shape analysis.

Keywords Cavitation cloud · Image processing · Shedding frequency · Two-phase flow · Cavitating jet

1 Introduction

Cavitation is a vapourization process that can happen without introducing heat into the system. It occurs when the local static pressure in a fluid reaches a level below the vapour pressure of the liquid at the actual working temperature. According to the Bernoulli equation, this may happen when a fluid accelerates in a pipe or around a pump impeller; thus,

cavitation is a common problem in fluidic equipment, such as pumps and control valves, causing serious wear, tear and damage. Under the wrong conditions, cavitation can reduce the lifetime of these components dramatically or can cause a drop in performance, high vibration and noise in hydraulic systems. On the other hand, the destructive power of cavitation can be deliberately used to modify and enhance the surface or mechanical properties of target materials, e.g. for cleaning, cutting or peening with relatively low energy consumption. Cavitating water jets have received much attention also in the environmental industry for the possibility to use them for the decomposition of toxic substances and the water treatment [1–8].

To prevent cavitation from negatively effecting hydraulic system performance or components, or to effectively use it for surface modification purposes, the investigation of this phenomenon and the study of its dynamics are essential. Until now, many experimental studies on cavitating water jets have been made concerning jet driven pressure, shape and size of a nozzle and cavitation number [7–14]. However, the structure of the cavitating jet and the behaviour of the unsteady cavitation bubbles are still in question, mostly due to the difficulty observing the interior of cavitating flows [15, 16]. With the purpose of performance prediction and efficient design of many

Technical Editor: Jader Barbosa Jr., Ph.D.

✉ Ezddin Hutli
ezddinhutli@yahoo.com

¹ Institute of Nuclear Techniques, Budapest University of Technology and Economics, Budapest, Hungary

² Department of Thermohydraulics, Centre for Energy Research, Hungarian Academy of Sciences, Budapest, Hungary

³ Energy Engineering Department, Faculty of Mechanical Engineering, Budapest University of Technology and Economics, Budapest, Hungary

⁴ Faculty of Mechanical Engineering, University of Belgrade, Belgrade, Serbia

⁵ Department of Electronics Technology, Budapest University of Technology and Economics, Budapest, Hungary

engineering devices such as turbomachinery, turbo-pumps in rocket propulsion systems, hydrofoils, fuel injectors, marine propellers, nozzles and cavitating jet generators, recently attention has also been focused on the numerical simulation of cavitating flows [17–21].

In this paper, high-speed photography was used to investigate and analyse the cavitation phenomenon, which was created by a high-speed submerged cavitating jet generator. Digital image processing was used to study the clouds' behaviour and structure and to measure parameters which can be used to characterize the system in function of the applied working conditions. The obtained results were statistically analysed both in time and in frequency domains. Considering a statistically relevant amount of data, besides the natural variation in the data set originating from the nature of this turbulent two-phased flow, the characteristic features of the cavitating jets can also be obtained. The shedding and discharging of the clouds can be considered a deterministic phenomenon, with certain characteristic frequencies superposed on the data set, which are depending on the hydrodynamic and geometrical working conditions, as it was discussed in previous publications. There are several formulas which can be used to calculate these frequencies. However, during the short time from shedding to discharging, cavity clouds are exposed to many forces originating from the turbulent interactions with the surrounding liquid in this complex, two-phase flow. Due to these forces, the behaviour and geometrical characteristics of the clouds cannot be easily predicted in time [9, 10, 15, 16, 22–27]. The statistical analysis of these geometrical parameters of the clouds (thickness, length, area) and their correlation with the working conditions can lead us to understand the cavitation phenomenon better and help us to enhance the performance of cavitating jet systems.

In time domain, the variation in the clouds' thickness and the area was investigated in function of time, the mean, standard deviation, skewness and kurtosis of their distributions were used to analyse the behaviour of the jet. In the frequency domain, fast Fourier transformation (FFT) was used to obtain the amplitude spectra based on the varying cloud areas and determine the characteristic frequencies of their dynamics. Through this image analysis, it is possible to quantitatively estimate the high-speed behaviour of the clouds, such as their consecutive shedding and discharging or other smaller processes, which take place before, in-between, or after these two main processes, such as shrinking, growing, re-entrant flow and pressure wave formation. It should be noted that the shedding and discharging processes are the main parameters for understanding the behaviour and performance of cavitating jet generators and other cavitating systems; thus, we will focus our investigation on these.

2 Experimental

2.1 Measurement set-up and procedure

The main part of the experimental set-up for our investigations is a high-speed submerged cavitating water jet generator, which consists of two connected closed hydraulic loops schematically depicted in Fig. 1. The chamber is first filled up with water, and then the plunger pump pressurizes the water. The high-speed submerged cavitating jet is generated in the thick-walled steel test chamber by the adjustment of appropriate hydrodynamic conditions. The final outflow arrives in the test chamber through the nozzle. For material testing purposes and for testing the performance of the cavitating jet generator, the specimens are mounted in the rotatable sample holder in a way that the tested specimen is coaxial with the nozzle. Essential components of the cavitating generator are the pressure and temperature sensors and the cooling system, which is connected to a temperature regulator, regulating valves, energy destructor and filters. More information regarding the test chamber can be found in our previous publications [28].

2.2 Visualization of the cavitating jets

A Photron APX ultra-high-speed camera (up to 100.000 frames/s) with a CORODIN 359-type flash lamp system was designed to operate the lamp with pulse durations of 0.5 to 11 ms. The system is triggered by a 30 V signal coming from the pulse generator. The test chamber has three transparent windows to be able to visualize the cavitating jet. In the test system, the light to the downstream chamber was supplied through two coaxial windows and the observation with the camera was done through the third window. To maximize the gathered light scattered from the cavities, the camera was mounted in such way to have free movement in any direction. The schematic components of the complete visualization system are shown in Fig. 2.

For the sake of clarity, the term cavity shedding refers to the moment when a new cavity starts at the lip of the nozzle, while the term discharging represents the break-off moment of the cavity. As discussed in previous publications, the shedding and discharging moments are periodical in nature and are very close to each other, so practically only one (the same) characteristic frequency describes this phenomenon [15]. The photographs of Fig. 3a, b illustrate the appearance and the shedding/discharging of the cavities. The numbers in Fig. 3b mark the shedding process of the cavitation clouds; in this way, the life of the clouds can be traced from shedding to discharging. Table 1 collects the working conditions for the experiments.

Fig. 1 **a** Schematic diagram of the cavitating jet generator (old version) (1—plunger pump, 2—filter, 3—regulating valve, 4—temperature sensor, 5—high-pressure transducer, 6—test chamber, 7—low-pressure transducer, 8—safety valve, 9—tank, 10—circulation pump, 11—heat exchanger, 12—energy dissipater, 13—pressure gauge, 14—flow indicator). **b** Schematic diagram of a typical nozzle. In our experiments, the actual outer diameter was 1 mm for the divergent direction and 0.45 mm for the convergent. **c** The schematic of the test chamber

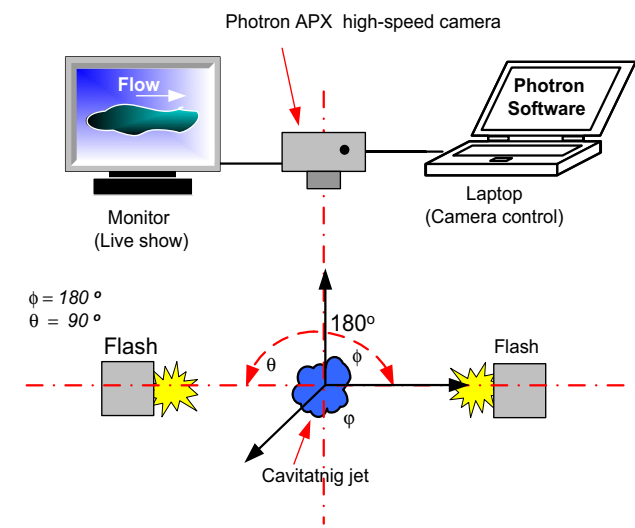
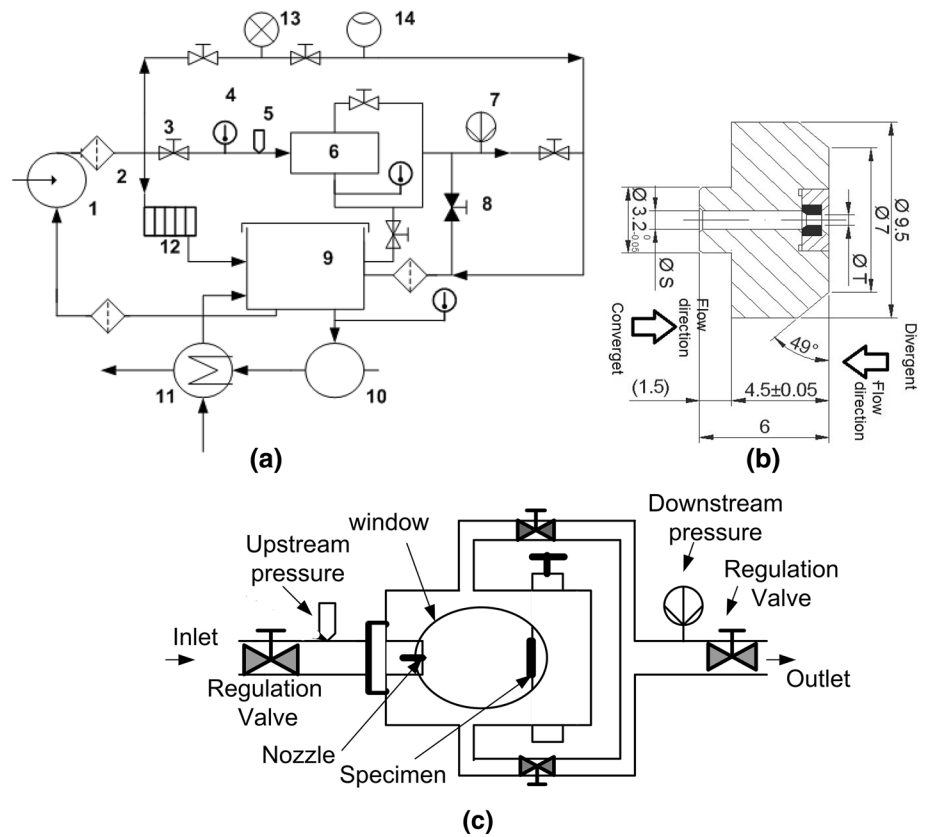


Fig. 2 Components of the high-speed cavity visualization test system

2.3 Digital image processing

Digital image processing, implemented in a custom MATLAB program, was used to identify and analyse the cavitation clouds based on the obtained photographs. The most important part of this sequence is the edge detection, which was carried out on binarized (grayscale) images. We used

the Canny edge detection algorithm, supported by the Otsu double thresholding method to extract the contour of the cavitation clouds and separate them from the background. The main steps of the autonomous image processing and subsequent evaluation programme are the following:

Step 1 Edge detection based on the Canny method. This step includes the determination of region of interest (ROI), conversion to grayscale, histogram-stretching (contrast optimization) noise removal (smoothing by applying Gaussian blur to the image) and the multi-stage edge detection algorithm. The latter uses gradient mapping; the local maxima in the gradient map is evaluated with edge tracking and double thresholding (Otsu method) to find the contour of the cavities.

Step 2 Cloud recognition by homogeneity testing: dividing the image into blocks that are more homogeneous than the image itself. This technique reveals information about the structure of the image and along with the detected edges enables the identification of coherent clouds (blocks), as shown in Fig. 4b.

Step 3 The measurement of cloud properties. The parameters are calculated at pixel level, as shown in Fig. 4c. For this exact same image, the results are given in Table 2.

Step 4 Cloud dynamics—Obtaining information about the strength and compactness of objects through image dynamics examination at the pixel level, including structure

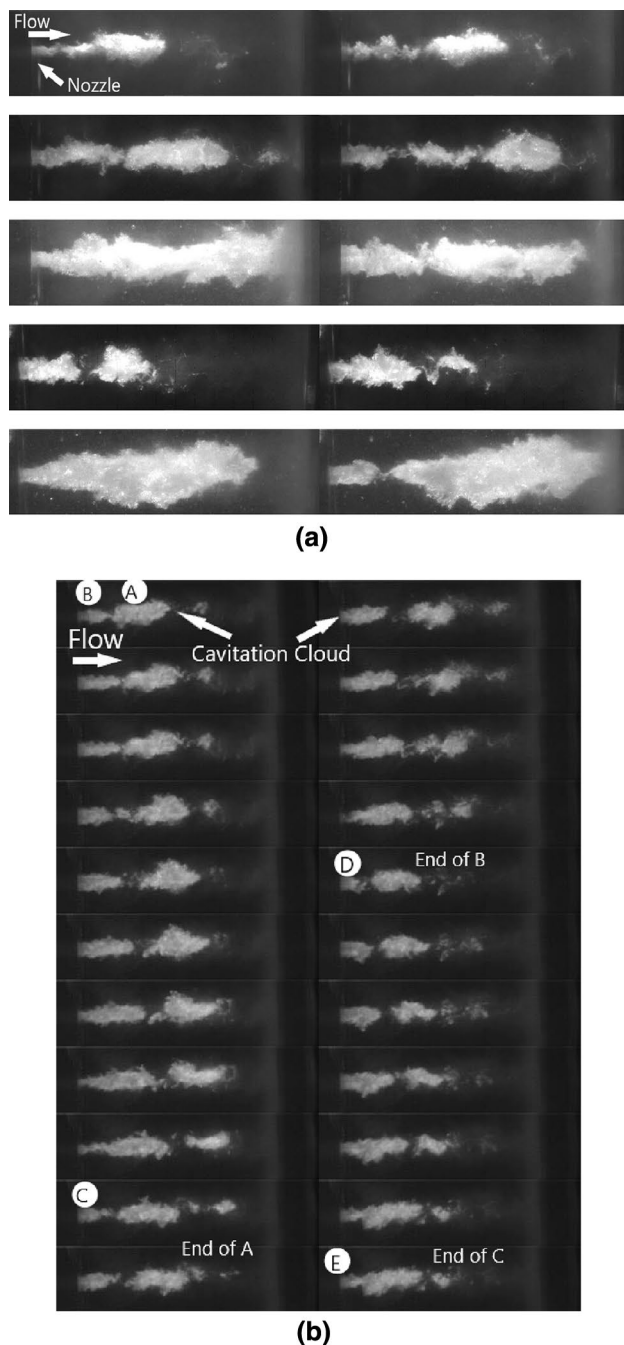


Fig. 3 Photographs from the appearance of the cavities—illustration of the influence of hydrodynamic and geometrical conditions. **a** From top to bottom: $P_1=105$ bar, 125 bars, 177 bars (for a convergent nozzle with a diameter of 0.45 mm), and 90.5 bar and 267 bars (for a divergent nozzle with a diameter of 1 mm). Frame rate 24.000 f/s, resolution 512×128 . **b** Illustration of the cavity shedding and discharging process for five cavity clouds (A, B, C, D, E) $P_1=105$ bar, frame rate 50.000 f/s, resolution 256×64 . For the detailed experimental conditions, please see Table 1

analysis within the object or pixel intensity or colour variations (Fig. 6).

Step 5 Analysis of the cloud thickness and the area in function of time at certain grid locations along the jet path (64, 128, 192, 256 and 320 pixels, corresponding to around 3.6 mm, 7.24 mm, 10.86 mm, 14.48 mm and 18.1 mm measured from the nozzle). An example of the cloud thickness variation in function of time is shown in Fig. 5.

2.4 Statistical analysis parameters

In our investigation, four main geometrical parameters were obtained and analysed: cloud thickness, area of the first cavity cloud (referred to as ‘area_first’, the cloud which is closest to the nozzle, currently under shedding), the areas of all the clouds together in one frame (referred to as ‘area_sum’), and the centre of mass. Besides the mean and standard deviation, the skewness and kurtosis of these parameters were also calculated as defined by Eqs. 1 and 2, respectively (where N is the sample size, x_i is the i th value, \bar{x} is the mean and σ is the standard deviation):

$$S_{sk} = \sum_{i=1}^N \frac{(x_i - \bar{x})^3}{N\sigma^3} \quad (1)$$

$$S_{ku} = \sum_{i=1}^N \frac{(x_i - \bar{x})^4}{N\sigma^4}. \quad (2)$$

In statistics, skewness is a measure of the asymmetry of the probability distribution of a real-valued random variable. Generally, a distribution has a positive skew (right-skewed) if the right tail is longer and negative skew (left-skewed) if the left tail is longer. When graphs are skewed, the median and mean are no longer equal. This parameter could be a good indicator for jet performance; as we will see later, to have a good performance of the cavitating jet generator data with positive skewness are preferred. Kurtosis is a measure of the relative peakedness of the distribution. Data sets with high kurtosis tend to have a distinct peak near the mean and decline rather rapidly. Data sets with low kurtosis tend to have a flat top near the mean rather than a sharp peak [29, 30]. To have good jet performance, data sets with high kurtosis would be preferred.

3 Results and discussion

3.1 The dynamic behaviour of the cavitation clouds

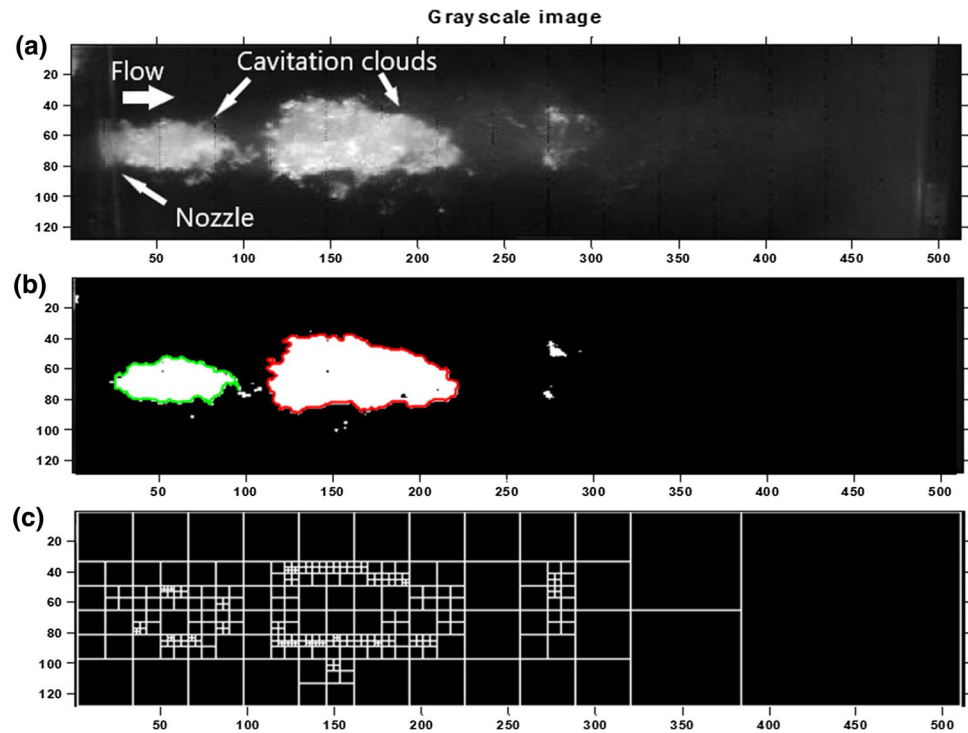
The behaviour of the clouds inside a cavitating jet is a fast and dynamic phenomenon. As an illustration, Fig. 6 shows

Table 1 Experimental conditions of the investigations

Nozzle shape (diameter [mm])	P_1 [bar]	P_2 [bar]	V_j [m/s]	σ [-]	K [-]	t_p [μ s]	f [s^{-1}]
Convergent (0.45)	105	2.06	96.5	0.022	0.0154	158	6335
Convergent (0.45)	125.7	2.06	105.4	0.019	0.0154	170	5810
Convergent (0.45)	177	2.06	125.7	0.013	0.0154	205	4880
Divergent (1)	90.5	1.89	22.8	0.34	0.0147	140	7140
Divergent (1)	267	1.89	39.35	0.11	0.0147	240	4170

The given shedding frequencies are analytically calculated

Fig. 4 **a** The original, grayscale photograph before processing. **b** The image after edge detection and cloud contour recognition. Note that small areas, which do not meet the size or homogeneity criterion, are rejected. **c** Measurement of cloud parameters at pixel level in the relevant areas. The scale is in pixels, which corresponds to 56.6 μ m

**Table 2** Obtained parameters of the two detected cavities from Fig. 4

Cloud number (contour)	Width [pixel]	Height [pixel]	Area [pixel ²]
1 (green)	73	33	1538
2 (red)	112	53	4124

The gap between the clouds = 27 pixel

A pixel corresponds to 56.6 μ m

a group of processed images (consecutive frames) of such cavitation clouds, where the colour scale corresponds to the light intensity of the original photographs. The internal structure of the cavities can be visualized by image examination on a pixel level, as presented in this figure. Based on these images, the dynamic behaviour of the clouds in space and time can be qualitatively determined and could

be used as indicator for their strength and compactness. As it can be seen in the images, the cloud is a living entity, and its own internal structure is governed by background processes. The dynamic of the whole jet can be followed by observing the consecutive frames. The projected 2D shape of the clouds is changing dynamically, which can be attributed to many reasons. Firstly, the shape and geometry of the clouds are related to their composition (vapour and liquid); secondly, the surface of the clouds can be considered quite rough (in three dimensions) due to the two-phase interactions and shear forces acting on the vapour–liquid interface. Since our presented method is technically using the light reflection of the vapour phase to image the clouds, this rapidly changing interface and randomly diffused light on the smaller bubbles can make the precise determination of the clouds' contour hard. Since this contour is distinguished based on the pixel intensity (via thresholding), the interface results in grey areas and thus the movement of the liquid

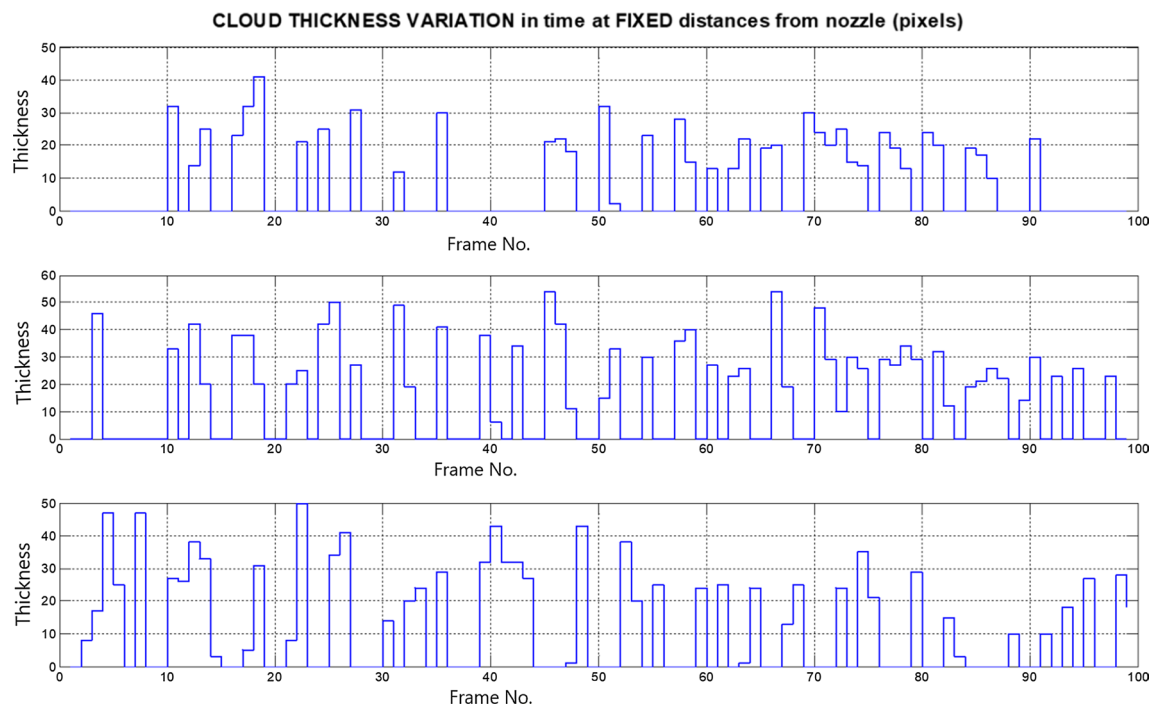


Fig. 5 An example for cloud thickness variation in time, measured at three fixed points, from top to bottom at 64, 128 and 192 pixels, corresponding to around 3.6 mm, 7.24 mm and 10.86 mm, respectively, measured from the lip of the nozzle

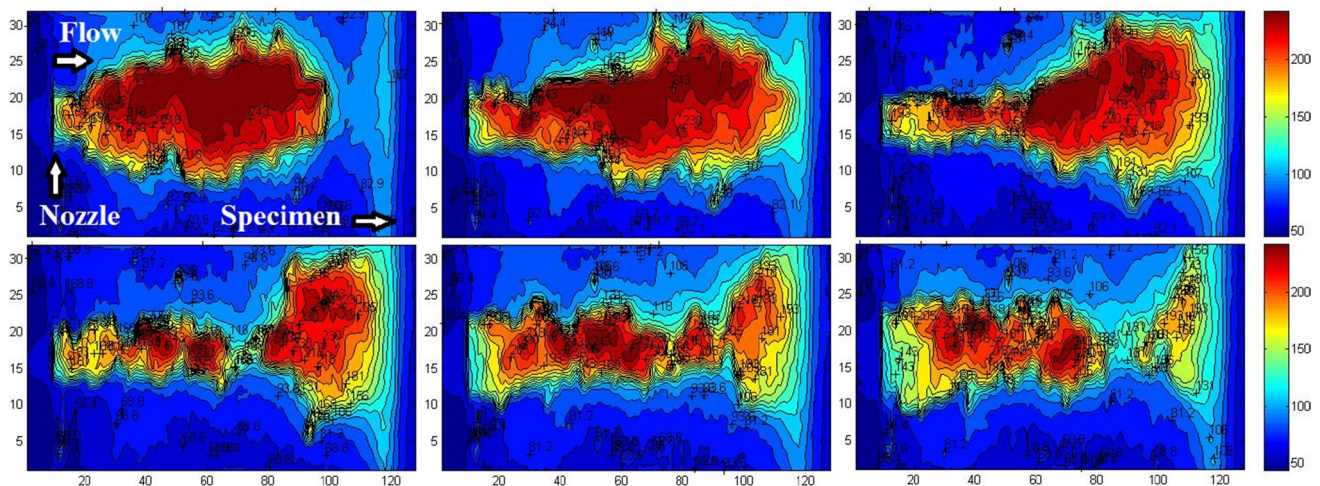


Fig. 6 2D consecutive images illustrating the strength and compactness of cavitation clouds realized through photography and image processing. The images show how the shape of the bubbles changes during the flow. Experimental conditions: $P_1=177$ bar, $P_2=2.06$ bar,

$V_j=125.7$ m/s, $\sigma=0.026$, $T=20$ °C, consecutive frame exposure time= $42\ \mu\text{s}$. The XY scale is in pixels, which corresponds to $56.6\ \mu\text{m}$. The colour scale is arbitrary corresponding to the normalized intensity of the image

layers around the cavitation clouds can also be seen and followed. The borderlines between the cavitation clouds and other liquid layers have a serpentine shape. This shape is a result of vortices originating from the turbulent movement of the jet, in addition of the compressing and expanding processes of the cavitating jet, which creates the shedding,

rebounding, collapsing (discharging) of the clouds, in addition to the micro-jets and shock waves. As the high-speed photographs of Figs. 7 and 8 present, the collapse of the bubbles can happen anywhere along the jet trajectory and a bubble may collapse on its own (Fig. 8/a) or after combining with another bubble (Fig. 8/b). The red arrows in Fig. 8

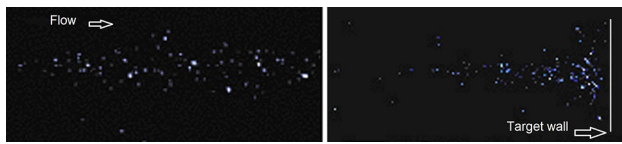


Fig. 7 Photographs of luminescent clouds in a cavitating jet. The bubble collapsing process along the jet trajectory and near/on target wall (specimen surface) can be followed this way. More information in [32]. (Experimental conditions: $P_1=213$ bar, $V_j=173$ m/s, $T=22$ °C)

indicate the micro-jets which are formed during these processes. This also supports that micro-jet can be formed even before the cavity bubble reaches the surface.

Tracing the life cycle of one cavitation cloud from its shedding to its discharging shows that after shedding the collapse (or degradation stage) of the cloud to small fragments might happen before or after its impact on the surface of the sample at the end of its trajectory. Both the characteristics and the time needed for the cloud to complete its life cycle are depending on the geometrical and hydrodynamic

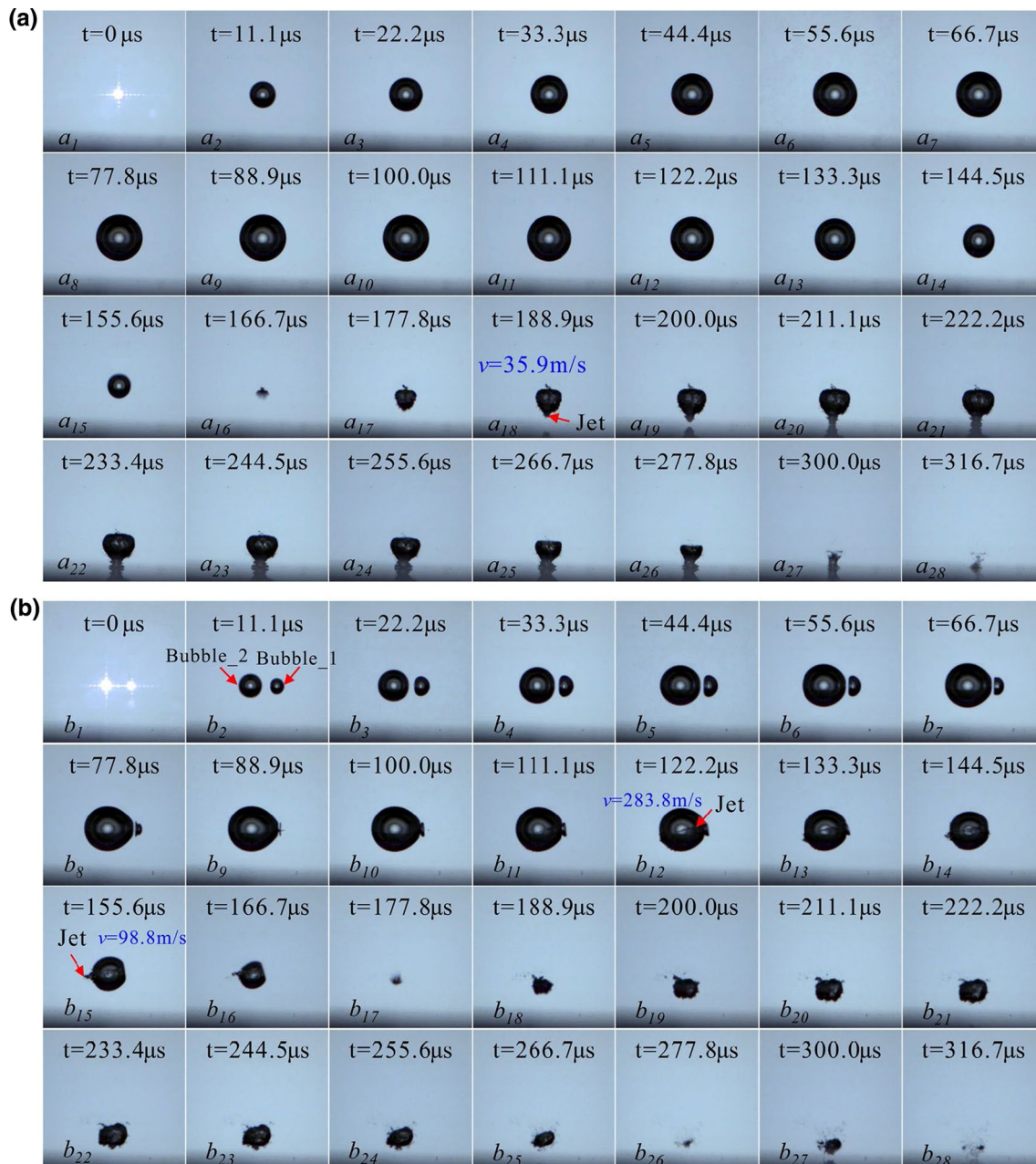


Fig. 8 High-speed photographs showing impact processes on target surfaces. Top set **a**: collapse of a single bubble. Bottom set **b**: collapse of two cavitation bubbles. More information in [34]. (Frame rate 180,000 fps, exposure time 2.50 μ s, frame width 5.45 mm)

working conditions. The evaluation of more than 1500 frames revealed that almost all cavities seldom maintain the axi-symmetric shape as moving downstream and often undergo a wavy deformation, probably reflecting the occurrence of the azimuthal instability of a vortex ring [31].

The analysis of the movies also shows that at low injection pressures (P_1) of 105 bar and 90.5 bar (convergent and divergent nozzle, respectively) the jet break-offs can be observed frequently, while at higher injection pressures (for both nozzle types) the jet break-off frequency decreased dramatically. At low injection pressures the instability could be attributed to the shortening of the vortex formation interval on the separated shear layer, or in other words the higher shedding frequencies can be related to the shorter length of the cavitating area and the created cavitation cloud has a less coherent structure compared to those created with higher injection pressures. The created cavities are not strong enough to sustain the effects of different forces which are acting on them in the turbulent flow field.

The cavities were found to persist downstream up to a certain value range of X/d (non-dimensional stand-off distance, where X is the distance between the nozzle and the target, and d is the nozzle diameter) [15, 32, 33]. This range depends on the factors mentioned earlier (hydrodynamic and geometrical conditions), but its precise determination was not the aim of our investigations.

3.2 Cavitation cloud thickness

In Fig. 3, we illustrated how the radial and axial expansions of the cavitation clouds are depending on both the geometric and hydrodynamic working conditions. An example in Fig. 5 presented the variation in cloud thickness in time, which showed that the clouds have a non-predictable, non-uniform shape, and their changing is related to processes such as shedding, growth, discharging, shrinking, regrowth and collapsing. These different processes are connected, and all of them have their own frequencies. Thus, the oscillation frequency of cloud thickness can be considered as a superposition of all these frequencies. These processes are also tightly connected to the injection pressure which has fluctuation depending on the frequency of the plunger pump ($f_{\text{pump}} = 3.77$ Hz).

Thus, the variation in the cloud's thickness can be considered as a good indicator to characterize their behaviour; hence, this was one of our main investigated parameters. Our custom MATLAB program was used to measure the cloud's thickness at five separate positions along the jet trajectory, as presented in Fig. 9a–e in the form of histograms, while Fig. 9f collects the mean and standard deviation of the whole data. The experimental conditions are given in Table 1.

Although the main running parameter is the injection pressure, please note that in two cases the nozzle geometry

was divergent with an outlet diameter of 1 mm (90.5 bar and 267 bar), while for three cases it was convergent with a diameter of 0.45 mm (105 bar, 125 bar, 177 bar). As we discussed in our previous publications, the nozzle geometry and diameter have a significant effect on the propagation distance, size of the cavitation clouds and actions, when the injection pressure and the flow rate are kept constant [9–11, 15, 32, 33]. As can be seen in Fig. 9, the closer the nozzle (position 1), the thicker the clouds produced by the divergent nozzles, while further away from the nozzle (positions 4 and 5) the thickness correlates with the injection pressure.

It can also be seen that the spread and standard deviation of the measured thicknesses both increase with the injection pressure and the position. At the first position, the thicknesses were between 0.1 and 3.2 mm, whose spread increased from 0.1 to 4.5 mm, 5 mm, 6 mm and 7 mm in the subsequent positions. As we go further downstream, the clouds are subjected more and more interactions, forces acting at the interface of the phases, which perturb their size [32, 33].

In the first measurement point, the thickness of the clouds shows a symmetric distribution for the divergent nozzle, for both injection pressures. For the convergent nozzle, $P_1 = 125$ bar resulted in a more symmetric distribution compared to the experiments with 105 bar and 177 bar. It is interesting that the maximum measured thickness was obtained with a convergent nozzle at 177 bar (3.6 mm), but as mentioned earlier the two divergent nozzles have higher average thicknesses at this position. The average values measured for the convergent nozzle correlate with the injection pressures (Fig. 9f). In the second measurement point, for both nozzle geometries, the average width increased for all injection pressures. The divergent nozzle has symmetric distribution, while the convergent has symmetric at 125 bar and non-symmetric at 105 and 177 bar pressures. In the third position, the divergent nozzle at 90.5 bar pressure still has the characteristic peak (most counts) at around 2.1 mm; however, the fact that the count of thicker clouds and the average thickness decrease may indicate the start of the disintegration process of the cloud. In contrast, the clouds generated with 267 bar are still developing, marked by the steady increase in the average thickness and a nearly ideal normal distribution. For the convergent nozzle, the thickness is increasing with the injection pressure, and the ideal distribution is still obtained with 125 bar. In the fourth position, the measured thickness for the divergent nozzle with 90.5 bar continues to decrease, confirming the disintegration of the cloud. For 267 bar, the thickness increases further, but the symmetry of the distribution is lost. For the convergent nozzle, the thickness still correlates with the pressure. In the final measurement point, the thickness measured for the 90.5 bar case drops drastically, meaning that the average penetration depth of the cavitating jet is smaller than measurement position, i.e.

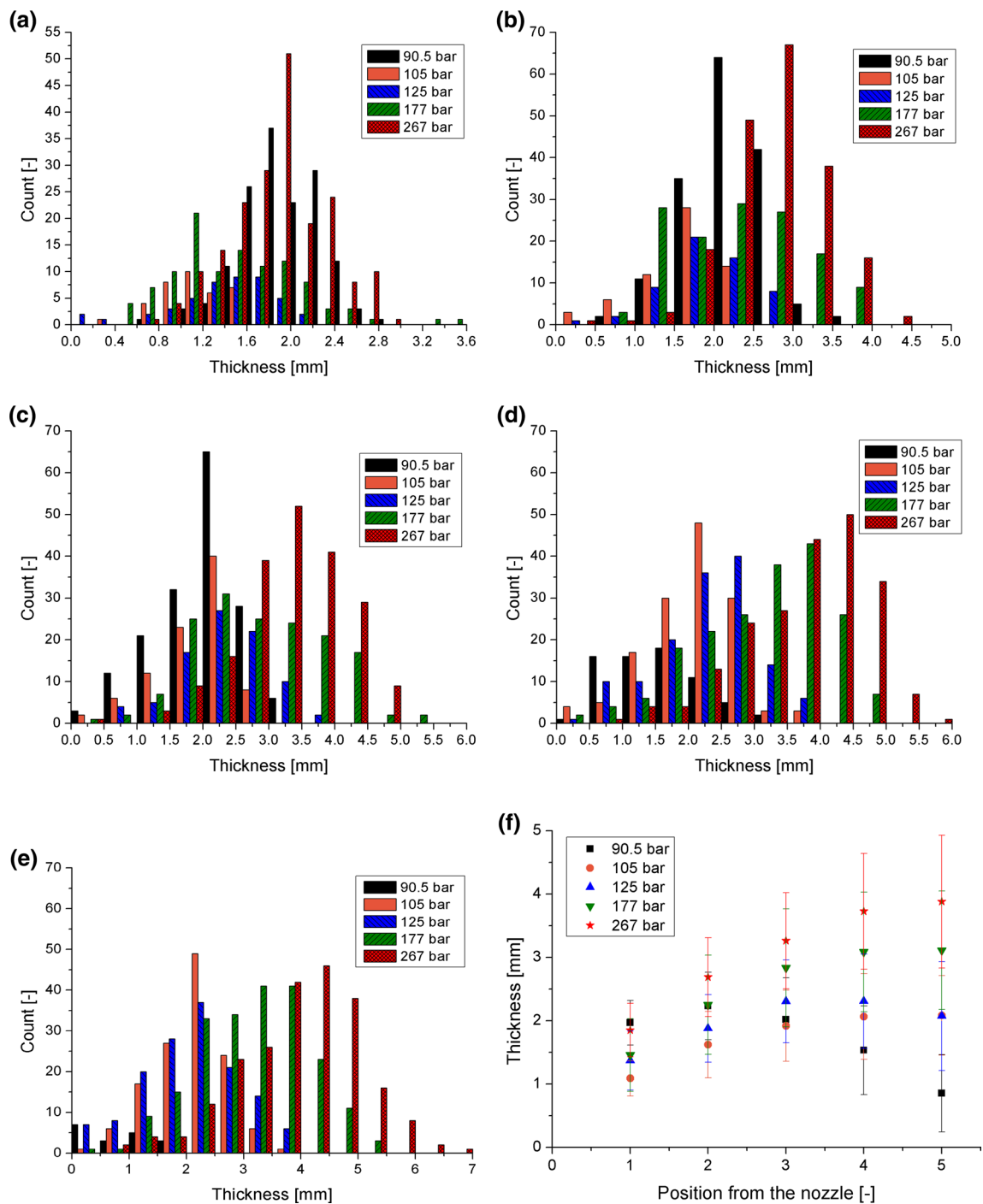


Fig. 9 a–e Histograms showing the distribution of the measured cloud thickness, measured in five positions, 3.6 mm, 7.24 mm, 10.86, 14.48 mm and 18.1 mm, starting from the nozzle inlet, for five injection pressures.

f Mean and standard deviation calculated on the data sets at the five positions

the cavity starts to vanish before this position. In the other hand, the jets with higher injection pressure (267 bar, 177 bar) reached a saturation stage, most perceivable in Fig. 9f.

Based on this analysis, we can say that the thickness can be used as a parameter to monitor the jet spreading angle and describe the shrinking, regrowth and collapsing processes

as well until the clouds completely vanish. As can be seen in Fig. 9f, for the divergent nozzle at 90.5 bar, the thickness only increases until the third measurement point, after which it starts to decrease. We can thus say that the penetration depth of the jet is close to this position, and the maximum spreading angle is here since the highest thickness

was measured here. While for the same nozzle at 267 bar, both the thickness and spreading angle continuously increase and reach saturation at around position 5. This indicates that the penetration depth of the jet under these working conditions is bigger than the available free distance (the distance between the nozzle and the target surface). For the convergent nozzle, the same process can be observed in function of the injection pressure. While at position 5 the thickness saturates at 177 bar, it shows a small decrease for lower pressures, e.g. for 125 bar.

Conclusively, we can state that regardless of the nozzle geometry, the cavitating jet thickness and spreading angle increase with the injection pressure and penetration.

Figure 10 presents the calculated kurtosis and skewness values for the thickness measurements. Although the data show significant variation, some tendencies, which characterize the above-discussed processes (Sect. 3.1), can be clearly seen. Looking at the data obtained for the experiment with 90.5 bar, we can see that the disintegration and later vanishing of the clouds are characterized by an abrupt drop in kurtosis and then a subsequent increase in the skewness. The drop in kurtosis means that there is no characteristic (dominant) thickness, while a positive skewness indicates a larger amount of thinner clouds, consistent with the vanishing. This process is also observable for the convergent nozzle at 125 bar (see also Fig. 9f). The data show a tendency for negative skewness except for the convergent nozzle at 177 bar, which shows some instability at the first few positions (see the double peaks in the histogram), and for the divergent nozzle at 90.5 bar in the vanishing phase. We can also say that well-developed jets have positive kurtosis, which indicates a strong, characteristic thickness.

Due to the nature of this highly turbulent, two-phase flow, the variation in the thickness of the clouds is high, and thus skewness and kurtosis did not yield much insight in this case. We will soon see that they will provide more

meaningful information when applied on the measured areas.

3.3 Cavitation cloud area

The longitudinal cross-sectional area of the cavitation clouds was also calculated with our custom MATLAB program. The resulting histograms for the areas of the first cloud (area_first) and all clouds on the photograph (area_sum) are shown in Fig. 11. Again, the nozzle geometry and diameter had a major impact on the measured area of the clouds: the divergent nozzle (with 1 mm outlet diameter) produces clouds with larger areas compared to the convergent nozzle (with 0.45 mm diameter), as can also be seen in the photographs of Fig. 3. Also, the area of the clouds strongly correlates with the applied injection pressure. The spread of the measured data, along with the standard deviation, also increases with the injection pressure, as shown in Fig. 11e.

By comparing the histograms of the first cloud's areas and summed cloud areas, we can gain information regarding the structure of the clouds. For the divergent nozzle, adding all the cloud fragments to the first cloud's area does not increase the average area much (Fig. 11e) compared to the convergent nozzle. This indicates that the clouds produced by the divergent nozzle have a more coherent structure—even if they are smaller and do not span to the whole length of the chamber as for 90.5 bar. For the convergent nozzle, the shape of the histogram changes significantly by summing all of the cloud fragments, compared to the first area, especially for smaller injection pressures the first clouds (area) will be smaller, indicating a more fragmented structure. The calculated kurtosis and skewness values are presented in Fig. 12. In the skewness values, we see a nice negative tendency with increasing injection pressure, especially for the summed areas. This is in good accordance with our previous observation that the

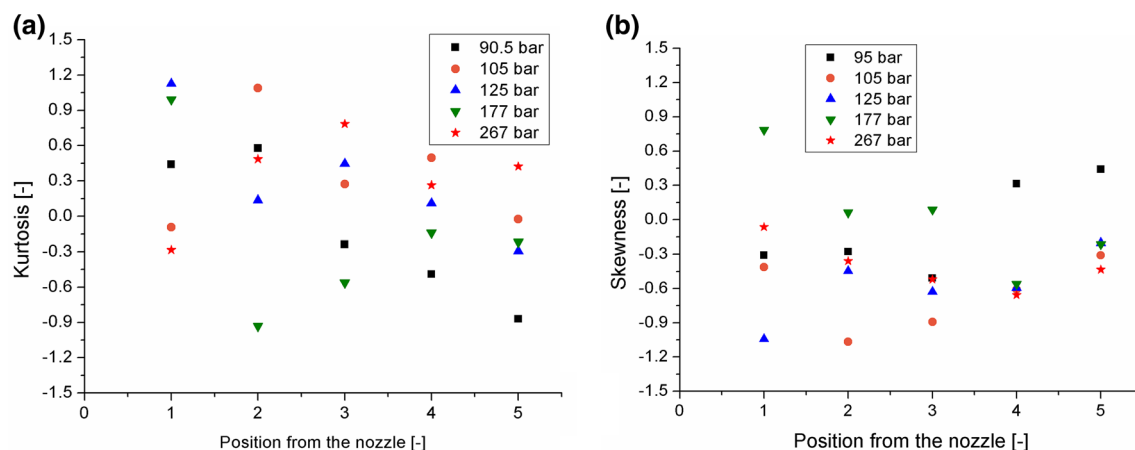


Fig. 10 **a** Kurtosis, **b** skewness of the thickness measurements at five different points along the jet trajectory for five injection pressures

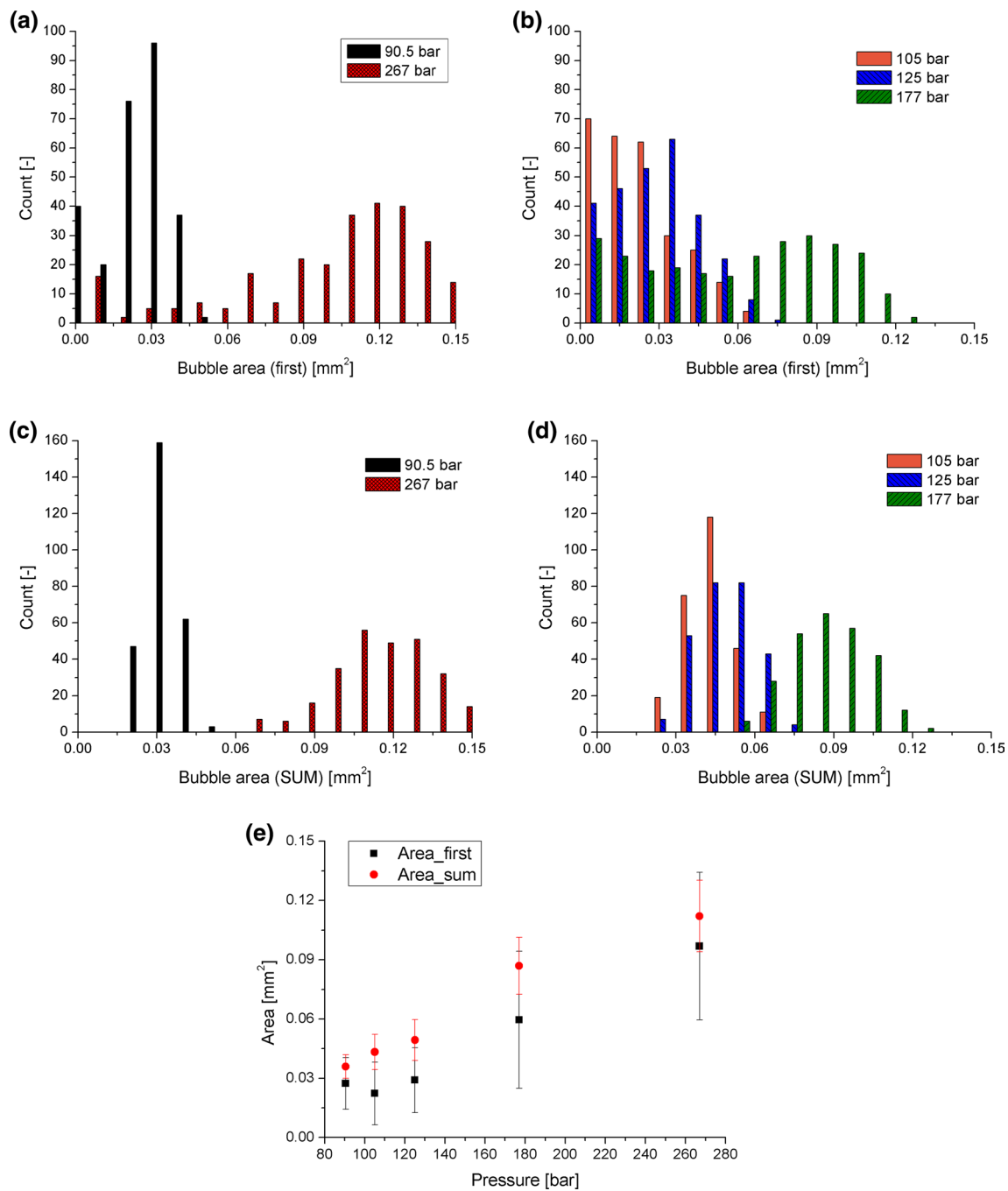


Fig. 11 a–d Histograms showing the distribution of the measured area of the cavitation clouds a, b first cloud in frame; c, d summed area of total clouds in. e Mean and standard deviation of area measurement

cloud size and penetration depth increase with injection pressure. Negative skewness indicates that larger clouds are more frequent in the distribution. The kurtosis values underline our other observation that the clouds produced with the divergent nozzle are more compact: the smaller, negative kurtosis measured for the convergent nozzle indicates a wider and flatter distribution, corresponding to less coherent clouds.

The cloud coherency can be attributed to the shedding frequency of the jet, which was found to be higher for the experiments performed with the convergent nozzle [9–11, 15, 32, 33]. Based on the determined cross-sectional area of the clouds, their volume can be estimated for the different experimental conditions. As it was discussed in our previous publication, the intensity of cavity collapse (i.e. the energy transferred during collapse) increases with larger cloud

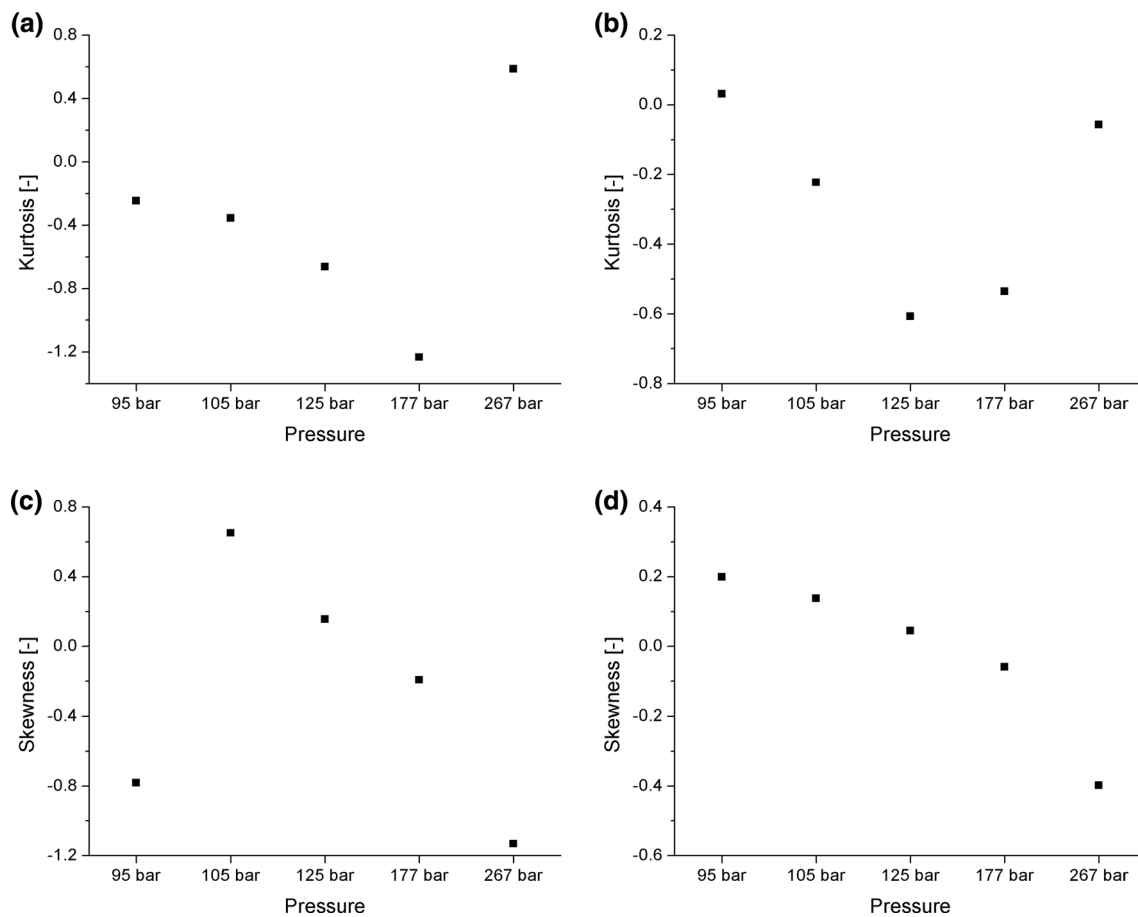


Fig. 12 a, b Kurtosis; c, d skewness of the area measurements presented in Fig. 11 for the area_first (left column) and area_sum (right column) histograms

volumes. At the same hydrodynamic working conditions, the convergent nozzle produces slender jets (with smaller thickness and area, i.e. less volume) in comparison with cavitating jets produced by the divergent nozzle. Its effectiveness was still found to be better because of the higher shedding frequency [9–11, 15, 22, 23]. Conclusively, our presented results are in good accordance with the mentioned previous observations.

3.4 Frequency domain analysis: pulsation frequency

In order to investigate the fluctuation in the area of the cavitation clouds, the Fourier spectra of the area data—obtained with 42 μ s time resolution between the consecutive frames—were calculated through fast Fourier transformation (FFT). The plots of Fig. 13 compare the resulting spectra for the different working conditions. The FFT spectra calculated for the first cloud's area (a), the summed area of all the clouds (b), and the position of the centre of mass along the longitudinal dimension (c) are also given.

It is important to be emphasized that these spectra characterize the oscillation frequency of the clouds, which is not to be confused with the shedding frequency. As discussed previously and in other papers, increasing injection pressures (or increasing Reynolds number) causes a drop in shedding frequencies [15, 26]. Here, the characteristic oscillation frequencies are found to increase with the injection pressure. As can be seen, at the lowest injection pressure of 90.5 bar there are barely a few peaks in the noise, while at higher pressures dominant frequencies emerge. Comparing the three injection pressures used with the convergent nozzle, we can see an increasing trend in the position of characteristic peaks in Fig. 13b. Dominant lower frequencies obtained for 267 bar can be accounted for the differences in the convergent/divergent type of nozzle. However, it is interesting to see that there are characteristic peaks at the same frequencies for both convergent and divergent nozzles at higher pressures (e.g. the peak at 2775 Hz). Figure 13d compares the three different FFT spectra calculated for the same experiment (177 bar, convergent nozzle). It can be seen that there are clearly

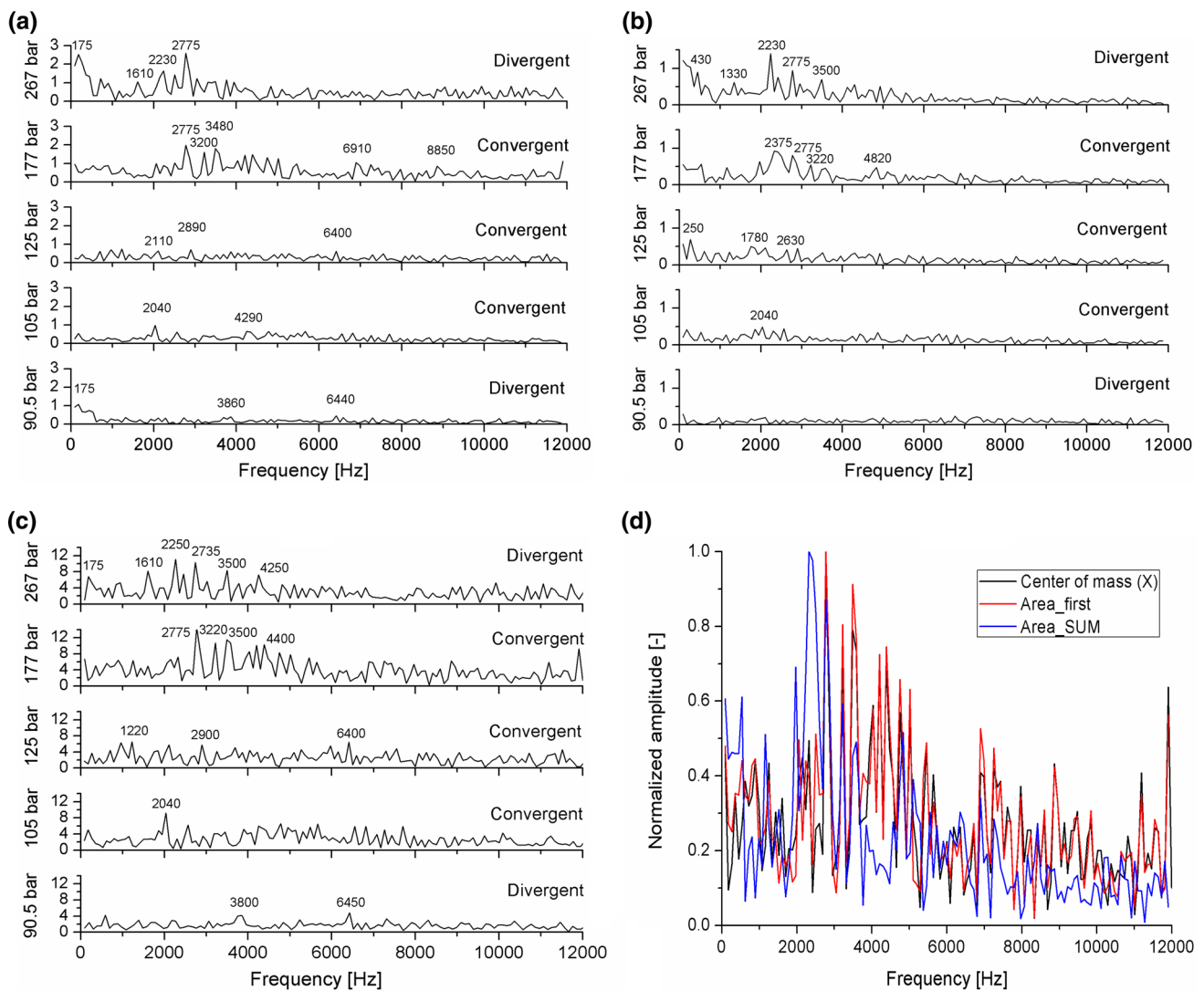


Fig. 13 FFT spectra of **a** the first cloud's measured area; **b** the summed area of the clouds; **c** the position of the cloud's centre of mass along the longitudinal dimension; **d** comparison of the three different FFT spectra for the data measured with the convergent nozzle at $P_1 = 177$ bar

overlapping peaks, especially between the FFT spectra calculated for the first area and the centre of mass (e.g. around 2775 Hz, 3200 Hz). Considering the summed area of the clouds, dominant peaks at slightly lower frequencies appear, around 2375 Hz. Comparing the three FFT spectra for the divergent nozzle at 267 bar, we can see that the characteristic peaks are much closer to each other, which again indicates that the coherency of the clouds is better compared to the convergent nozzle.

It is demonstrated that with our proposed image processing method it was possible to measure the oscillation frequency of the produced cavitation clouds, which was found to be characteristic in the 2–5 kHz range, depending on the working conditions. The appearance and position of these peaks yield useful information about the morphology of the clouds and the behaviour of the cavitating jet in general.

4 Conclusion

Image processing and statistical analysis were used to study the two-phase flow dynamic behaviour of cavitating flow issued using a high-speed cavitating water jets generator. The thickness and area of the clouds and their oscillation frequency (based on the changes in their area and centre of mass) were used to study their morphology in function of the working conditions, mainly nozzle type (convergent, divergent) and injection pressure. The results show that by increasing the injection pressure, the penetration depth and total area of the cavitation clouds increase, and the resulting clouds are better developed with an increasing thickness along their path. It was also found that the divergent nozzle produced more coherent clouds compared to the convergent nozzle. The FFT analysis

showed that at higher injection pressures (above 125 bar) characteristic peaks appear in the oscillation frequency of the clouds, which are most dominant in the 2–5 kHz range. Conclusively, it was demonstrated that the introduced image processing method is a useful tool to study the behaviour of cavitation clouds in detail, which can help in their further optimization for various applications.

Acknowledgements Open access funding provided by Budapest University of Technology and Economics (BME). The first author would like to express his gratitude to the Ministry of Science in Libya, for support through his research activity and the Libyan Ministry of higher education, who paid EPFL-LMH for using the facility. The authors are grateful for the help of Prof. Petar B. Petrović from Faculty of Mechanical Engineering, University of Belgrade (Serbia), for the MATLAB software used partially here. The research reported in this paper was partially supported by the Higher Education Excellence Program of the Ministry of Human Capacities in the frame of Nanotechnology and Materials Science research and also Biotechnology research areas of Budapest University of Technology and Economics (BME FIKP-NAT and BME FIKP-BIO).

Open Access This article is distributed under the terms of the Creative Commons Attribution 4.0 International License (<http://creativecommons.org/licenses/by/4.0/>), which permits unrestricted use, distribution, and reproduction in any medium, provided you give appropriate credit to the original author(s) and the source, provide a link to the Creative Commons license, and indicate if changes were made.

References

- Soyama H (2017) Key factors and applications of cavitation peening. *Int J Peen Sci Technol* 1:3–60
- Dular M et al (2016) Use of hydrodynamic cavitation in (waste) water treatment. *Ultrason Sonochem* 29:577–588
- Dindar E (2016) An overview of the application of hydrodynamic cavitation for the intensification of wastewater treatment applications: a review. *Innov Energy Res* 5:137–144. <https://doi.org/10.4172/2576-1463.1000137>
- Yunfeng Xu, Yang J, Wang Y, Feng L, Jinping J (2006) The effects of jet cavitation on the growth of *Microcystis aeruginosa*. *J Environ Sci Health Part A* 41:2345–2358
- Yusof NSM, Babgi B, Alghamdi Y, Aksu M, Madhavan J, Ashokkumar M (2016) Physical and chemical effects of acoustic cavitation in selected ultrasonic cleaning applications. *Ultrason Sonochem* 29:568–576. <https://doi.org/10.1016/j.ultsonch.2015.06.013>
- Filho JGD, Assis MP, Genovez AIB (2015) Bacterial inactivation in artificially and naturally contaminated water using a cavitating jet apparatus. *J Hydro-Environ Res* 9:259–267. <https://doi.org/10.1016/j.jher.2015.03.001>
- Hutli E, Nedeljkovic M, Bonyár A, Radovic N, Llic V, Debeljkovic A (2016) The ability of using the cavitation phenomenon as a tool to modify the surface characteristics in micro and in nano level. *Tribol Int* 101:88–97
- Hutli E, Nedeljkovic M, Bonyár A (2018) Controlled modification of the surface morphology and roughness of stainless steel 316 by a high speed submerged cavitating water jet. *Appl Surf Sci* 458:293–304
- Hutli E, Nedeljkovic M, Radovic N, Bonyár A (2016) The relation between the high speed submerged cavitating jet behaviour and the cavitation erosion process. *Int J Multiph Flow* 83:27–38
- Hutli E, Nedeljkovic M, Bonyár A, Légrády D (2017) Experimental study on the influence of geometrical parameters on the cavitation erosion characteristics of high speed submerged jets. *Exp Thermal Fluid Sci* 80:281–292
- Hutli E, Nedeljkovic M, Bonyár A (2018) Cavitating flow characteristics, cavity potential and kinetic energy, void fraction and geometrical parameters—analytical and theoretical study validated by experimental investigations. *Int J Heat Mass Transf* 117:873–886
- Soyama H (2013) Effect of nozzle geometry on a standard cavitation erosion test using a cavitating jet. *Wear* 297:895–902. <https://doi.org/10.1016/j.wear.2012.11.008>
- Chi P, Shouceng T, Gensheng L (2016) Joint experiments of cavitation jet: high-speed visualization and erosion test. *Ocean Eng* 149:1–13
- Madadnia J, Shanmugam DK, Nguyen T, Wang J (2008) A study of cavitation induced surface erosion in abrasive water jet cutting systems. *Adv Mater Res* 53–54:357362
- Hutli E, Nedeljkovic M (2008) Frequency in shedding/discharging cavitation clouds determined by visualization of a submerged cavitating jet. *J Fluids Eng ASME* 130:8. <https://doi.org/10.1115/1.2813125>
- Guoyi P, Ayaka W, Yasuyuki O, Seiji S, Hong J (2018) Periodic behaviour of cavitation cloud shedding in submerged water jets issuing from a sheathed pipe nozzle. *J Flow Control Meas Vis* 6:15–26
- Ahuja V, Hosangadi A, Arunajatesan S (2001) Simulations of cavitating flows using hybrid unstructured meshes. *J Fluids Eng* 123:331–340
- Barre S, Rolland J, Boitel G, Goncalves E, Fortes PR (2009) Experiments and modelling of cavitating flows in venturi: attached sheet cavitation. *Eur J Mech B-Fluids* 28:444–464
- Guoyi P, Seiji S (2013) Progress in numerical simulation of cavitating water jets. *J Hydrodyn Ser B* 25:502–509. [https://doi.org/10.1016/S1001-6058\(11\)60389-3](https://doi.org/10.1016/S1001-6058(11)60389-3)
- Goncalves E, Patella RF (2009) Numerical simulation of cavitating flows with homogeneous models. *Comput Fluids* 38:1682–1696. <https://doi.org/10.1016/j.compfluid.2009.03.001>
- Barberon T, Helluy P (2005) Finite volume simulation of cavitating flows. *Comput Fluids* 34:832–858
- Shimizu S, Adachi H, Izumi K, Sakai H (2007) High-speed observations of submerged water jets issuing from an abrasive water jet nozzle. In: American WJTA conference and expo, organized and sponsored by the Water Jet Technology Association Houston, Texas, pp 1–15. <https://www.wjta.org/image/s/wjta/Proceedings/Papers/2007/H4%20shimizu.pdf>. Accessed 07 June 2019
- Soyama H, Yamauchi Y, Sato K, Ikohagi T, Oba R, Oshima R (1993) High-speed observation of ultra-high-speed cavitating submerged water jets. *Trans Jpn Soc Mech Eng Ser B* 59:3714–3719. <https://doi.org/10.1299/kikaib.59.3714>
- Keiichi S, Yasuhiro S, Saburo O (2009) Structure of periodic cavitation clouds in submerged impinging water-jet issued from horn-type nozzle. In: 9th Pacific rim international conference on water jetting technology. https://www.kanazawa-it.ac.jp/flab/database/paper/2009_PRIC-WJT2009.pdf. Accessed 07 June 2019
- Sato K, Taguchi Y, Hayashi S (2013) High Speed observation of periodic cavity behavior in a convergent-divergent nozzle for cavitating water jet. *J Flow Control Meas Vis* 1:102–107. <https://doi.org/10.4236/jfcmv.2013.13013>
- Satoshi N, Osamu T, Hitoshi S (2012) Similarity law on shedding frequency of cavitation cloud induced by a cavitating jet. *J Fluid Sci Technol JSME* 7:405–420
- Soyama H (2005) High-speed observation of a cavitating jet in air. *J Fluids Eng* 127:1095–1101

28. Hutli E, Nedeljkovic M (2008) Mechanics of submerged jet cavitating action: material properties, exposure time and temperature effects on erosion. *Arch Appl Mech* 78:329–341
29. Doane DP, Lori E (2011) Measuring skewness: a forgotten statistic. *J Stat Educ* 19:1–8
30. McNeese B (2016) Are the skewness and kurtosis useful statistics. <https://www.spcforexcel.com/knowledge/basic-statistics/are-skewness-and-kurtosis-useful-statistics>. Accessed 07 June 2019
31. Widnall SE, Sullivan JP, Owen PR (1973) On the stability of vortex rings. *Proc R Soc Lond A* 332:335–353
32. Hutli E, Alteash O, Ben Raghisa M, Nedeljkovic M, Ilic V (2013) Appearance of high submerged cavitating jet: the cavitation phenomenon and sono-luminescence. *Thermal Sci* 17:1151–1161
33. Hutli E, Abouali S, Ben Hucine M, Mansour M, Nedeljkovic M, Ilic V (2013) Influence of hydrodynamic conditions and nozzle geometry on appearance of high submerged cavitating jets. *Thermal Sci* 17:1139–1149
34. Jing L, Zhipan N (2019) Jet and shock wave from collapse of two cavitation bubbles. *Sci Rep* 9:1352–1365. <https://doi.org/10.1038/s41598-018-37868-x>

Publisher's Note Springer Nature remains neutral with regard to jurisdictional claims in published maps and institutional affiliations.